ISPRS Journal of Photogrammetry and Remote Sensing 172 (2021) 79–94

Contents lists available at ScienceDirect

ISPRS Journal of Photogrammetry and Remote Sensing

journal homepage: www.elsevier.com/locate/isprsjprs

Tropical forest canopy height estimation from combined polarimetric SAR and LiDAR using machine-learning

Maryam Pourshamsi [a,*,1], Junshi Xia [b], Naoto Yokoya [b], Mariano Garcia [c], Marco Lavalle [d], Eric Pottier [e], Heiko Balzter [a,f]

[a] School of Geography, Geology and the Environment, University of Leicester, University Road, Leicester LE1 7RH, UK
[b] Geoinformatics Unit, RIKEN Center for Advanced Intelligence Project (AIP), Japan
[c] Department of Geology, Geography and Environment, University of Alcalá, 28801 Alcalá de Henares, Madrid, Spain
[d] NASA Jet Propulsion Laboratory, California Institute of Technology, Pasadena, CA, USA
[e] Insitut d'Electronique et de Télécommunication des Rennes, University de Rennes 1, Rennes Cedex, France
[f] National Centre for Earth Observation, University of Leicester, University Road, Leicester LE1 7RH, UK

ARTICLE INFO

Keywords:
Polarimetric synthetic aperture radar (PolSAR)
LiDAR
L-band
Forest height
Machine learning

ABSTRACT

Forest height is an important forest biophysical parameter which is used to derive important information about forest ecosystems, such as forest above ground biomass. In this paper, the potential of combining Polarimetric Synthetic Aperture Radar (PolSAR) variables with LiDAR measurements for forest height estimation is investigated. This will be conducted using different machine learning algorithms including Random Forest (RFs), Rotation Forest (RoFs), Canonical Correlation Forest (CCFs) and Support Vector Machine (SVMs). Various PolSAR parameters are required as input variables to ensure a successful height retrieval across different forest heights ranges. The algorithms are trained with 5000 LiDAR samples (less than 1% of the full scene) and different polarimetric variables. To examine the dependency of the algorithm on input training samples, three different subsets are identified which each includes different features: subset 1 is quiet diverse and includes non-vegetated region, short/sparse vegetation (0–20 m), vegetation with mid-range height (20–40 m) to tall/dense ones (40–60 m); subset 2 covers mostly the dense vegetated area with height ranges 40–60 m; and subset 3 mostly covers the non-vegetated to short/sparse vegetation (0–20 m) .The trained algorithms were used to estimate the height for the areas outside the identified subset. The results were validated with independent samples of LiDAR-derived height showing high accuracy (with the average $R^2 = 0.70$ and RMSE = 10 m between all the algorithms and different training samples). The results confirm that it is possible to estimate forest canopy height using PolSAR parameters together with a small coverage of LiDAR height as training data.

1. Introduction

Forest height is a significant forest biophysical parameter which could be used to derive important information about forest ecosystems, such as forest above ground biomass (AGB). Remote sensing technologies offer different techniques for retrieval of this parameter including Light Detection And Ranging (LiDAR) and Polarimetric Interferometric Synthetic Aperture Radar (PolInSAR). LiDAR is able to measure the forest canopy height directly and it provides the most precise measurements in compare to other remote sensing techniques. The use of LiDAR data for forest canopy height mapping is well demonstrated and established in the literature (Dubayah and Drake, 2000, Simard et al., 2011, Fayad et al., 2016, Silva et al., 2018). Nevertheless, LiDAR availability, particularly on airborne platforms, is limited by the acquisitions cost and persistent cloud cover especially in the tropics. PolInSAR is a model-based technique for estimation of forest canopy height (Cloude and Papathanassiou, 1997, Cloude and Papathanassiou, 1998). It uses two polarimetric SAR (PolSAR) images that are acquired over a test site with a given temporal and spatial baselines. Besides the challenges associated with temporal and volume decorrelation (Kugler et al., 2015, Lavalle and Hensley, 2012) affecting the performance of PolInSAR model, current applications of PolInSAR are constrained by

* Corresponding author.
E-mail addresses: hb91@le.ac.uk (M. Pourshamsi), junshi.xia@riken.jp (J. Xia), naoto.yokoya@riken.jp (N. Yokoya), mariano.garcia@uah.es (M. Garcia), marco.lavalle@jpl.nasa.gov (M. Lavalle), eric.pottier@univ-rennes1.fr (E. Pottier), hb91@le.ac.uk (H. Balzter).
[1] Airbus Defence and Space, 60 Priestley Road, Guildford, Surrey, GU2 7AG, United Kingdom.

https://doi.org/10.1016/j.isprsjprs.2020.11.008
Received 20 May 2020; Received in revised form 13 November 2020; Accepted 15 November 2020
Available online 19 December 2020

the limited availability of spaceborne PolInSAR data (Pourshamsi et al., 2018a). Currently there are data sources from spaceborne SAR interferometers such as Sentinel-1A and B (C-band; (Torres et al., 2012), Tandem-X (X-band (Krieger et al., 2007), RADARSAT-2 (C-band; (Khati, et al., 2018)), and ALOS-PALSAR2 (L-band; (Shimada et al., 2014)). SAR C- and X-band are categorized as SAR short wavelengths and are not suitable for mapping forest height over tropical regions, because tropical forests are highly complex, dense and up to 70 m tall. Short SAR wavelengths do not penetrate into the canopy all the way to the ground; therefore, canopy height is generally underestimated unless a ground digital terrain model is available. Kugler et al., 2015 explored the suitability of the TanDEM-X PolInSAR data for forest height estimation for three different forest types, boreal, temperate and tropical. While the results are significantly accurate for the boreal ($R^2 = 0.86$) and temperate ($R^2 = 0.77$), it is less accurate for the tropical forest ($R^2 = 0.50$) (Kugler et al., 2015). This is due to the interaction of the X-Band SAR with the canopy leaves which causes a low penetration. RADARSAT-2 and Sentinel-1A and B offer a SAR C-Band which is again categorised as short SAR wavelength. Likewise X-Band SAR, it is also suffered by the canopy penetration capability for the tropical forest. In addition to this limitation, their data are acquired in a repeat-pass interferometric mode. Hence, their data are highly influenced by the volume and temporal decorrelations that significantly lead to a loss of coherence, which then cause a large bias in the height estimation of the tropical forest (Khati, et al., 2018). PolInSAR data from ALOS-PALSAR2 sensor are also available. However, similar to RADARSAT-2 and Sentinel-1A and B data, its data are acquired in a repeat-pass mode (Khati, et al., 2018).

Considering the issues associated with the current techniques for forest height estimation and the availability of the required data, there are needs for new approaches for forest canopy height estimation. An example is merging multi-source remotely sensed data such as PolSAR and LiDAR. PolSAR data provide important information about the physical scattering mechanisms (Lee and Pottier, 2009), but they do not allow direct retrieval of vertical scattering profiles. Hence, they should be combined with other data sources that provide vertical scattering profiles inside forest canopies such as LiDAR. This could be conducted in a machine learning approach. Therefore, in this study the potential of integrating PolSAR and sparse LiDAR datasets using machine learning algorithm for estimating tropical forest canopy height is demonstrated.

Recently, numerous machine learning algorithms methods have been used for combining multisource remotely sensed data due to accurate classification/regression capability, less parameter tuning and lower computational complexity, higher ability to integrate multisource data, or no assumptions made on the data distribution among others. The most popular and widely used machine learning methods are Decision Trees (DT) ensemble methods (e.g. Random Forest (RF)) and Support Vector Machine (SVM) (Smola and Schölkopf, 2004). DT ensembles capture non-linearity between predictors and response, and also deal with highly correlated features. They can run on large-scale datasets in an efficient way and are robust to outliers and noise.

SVM is a supervised classifier which explicitly looks for the best separating line (hyperplane) in the multi-dimensional dataset (Smola and Schölkopf, 2004) for both regression and classification tasks. The support vectors attempt to find an optimal regression that deviates from the target (training input) less that a given threshold ε while being as flat as possible (Smola and Schölkopf, 2004).

The applications of machine learning algorithms for merging multisource remotely sensed data for forestry applications have been well established and documented in the scientific literature. They cover various applications such as forest health (Wang et al., 2015), forest fire (Zhao et al., 2011), forest change (Singh et al., 2014), and forest biomass (Gleason and Im, 2012; Fassnacht et al., 2014), etc. Although there have been many studies focused on various forestry applications (e.g. forest biomass estimation) using machine learning, only a small attempt has been made for forest height estimation. Stojanova et al., 2010 investigated forest canopy height mapping by combining LiDAR and Landsat data using ensemble methods and single- and multi-target regression trees. Chen et al., 2012 suggested a joint use of LiDAR and Quickbird imagery in a Support Vector Regression (SVR) model to estimate forest canopy height over a test site in Quebec, Canada. Gu et al., 2018 explored forest height mapping using a combination of Geometric-Optical Model for Sloping Terrains (GOST), Landsat 7 ETM+, and airborne LiDAR in the western Greater Khingan Mountains of China using neural network and a look-up table. García et al. (2018) proposed a forest canopy height modelling technique by merging LiDAR, multispectral data and SAR backscatter using SVM where SAR backscatter and multispectral data were used to extrapolate LiDAR measurements and estimate forest canopy height at a larger scale. Li et al., 2020 proposed merging the ICESat-2 satellite LiDAR data with Sentinel-1 (SAR C-Band), Sentinel-2 (Optical) and Landsat-8 data using Deep Learning and Random Forest. Brigot et al., 2019 investigated the potential of fusing PolInSAR data with LiDAR height using Random Forest and Neural Network. Xie et al., 2019 proposed a multi-baseline PolInSAR and LiDAR data merging approach for improved forest height estimation. In a similar study, Pourshamsi et al. (2018a) examined an integration of PolInSAR components and LiDAR-derived height using SVM for improved estimation of forest height. Whilst the results obtained from this approach are more accurate than PolInSAR alone, the model performance is limited by the PolInSAR data availability. Pourshamsi et al., (2018b) investigated the combined use of polarimetric SAR parameters extracted from different decomposition techniques (H/A/Alpha (Cloude and Pottier, 1996) and Krogager (Krogager, 1990) and LiDAR samples to estimate forest height using SVM. The estimated height has a significant accuracy and is relatively similar to the one estimated by the PolInSAR technique (Pourshamsi et al., 2018c). Although their results are significant and showed the potential of the approach for accurate forest height estimation in the absence of interferometric measurements, the LiDAR samples for training the model were collected from all part of the scene. This large distribution of LiDAR samples overlapping the entire SAR image is not often available. This underlines the need for examination of the approach with a different data sampling scenario for training the model. Additionally, in their study only the performance of the SVM is assessed. So, there is a need to assess the effectiveness of the application (PolSAR and LiDAR data integration for forest height estimation) by examining it in different machine learning models.

This study aims at investigating the capabilities of PolSAR parameters extracted from different polarimetric decompositions for forest height estimation by combining them with LiDAR-derived height using different machine learning algorithms and extracting the training samples from a subset of the scene. This allowed investigating the dependency of the model performance on the training data. Multiple machine learning algorithms including Random Forest (RF), Rotation Forest (RoF), Canonical Correlation Forest (CCF) and Support Vector Machine (SVM) are used to extrapolate LiDAR-derived height using PolSAR parameters. This allowed checking PolSAR parameters capabilities for forest height estimation independent of the type of machine learning algorithms. The specific objectives of this paper are to 1) quantify the accuracy of forest canopy height retrieval integrating PolSAR-decomposition-based components with LiDAR samples; 2) explore the potential of PolSAR components for estimation of forest height in the absence of interferometric SAR measurements; 3) investigate the dependency of model performance on the training data and 4) explore the sensitivity of the input features to forest canopy height estimation. Presenting this method for integrating these multi-sensor datasets for forest height estimation, exploring the model dependency on the selected training data, and investigating the application performance across different machine learning models are the novel contribution of this research.

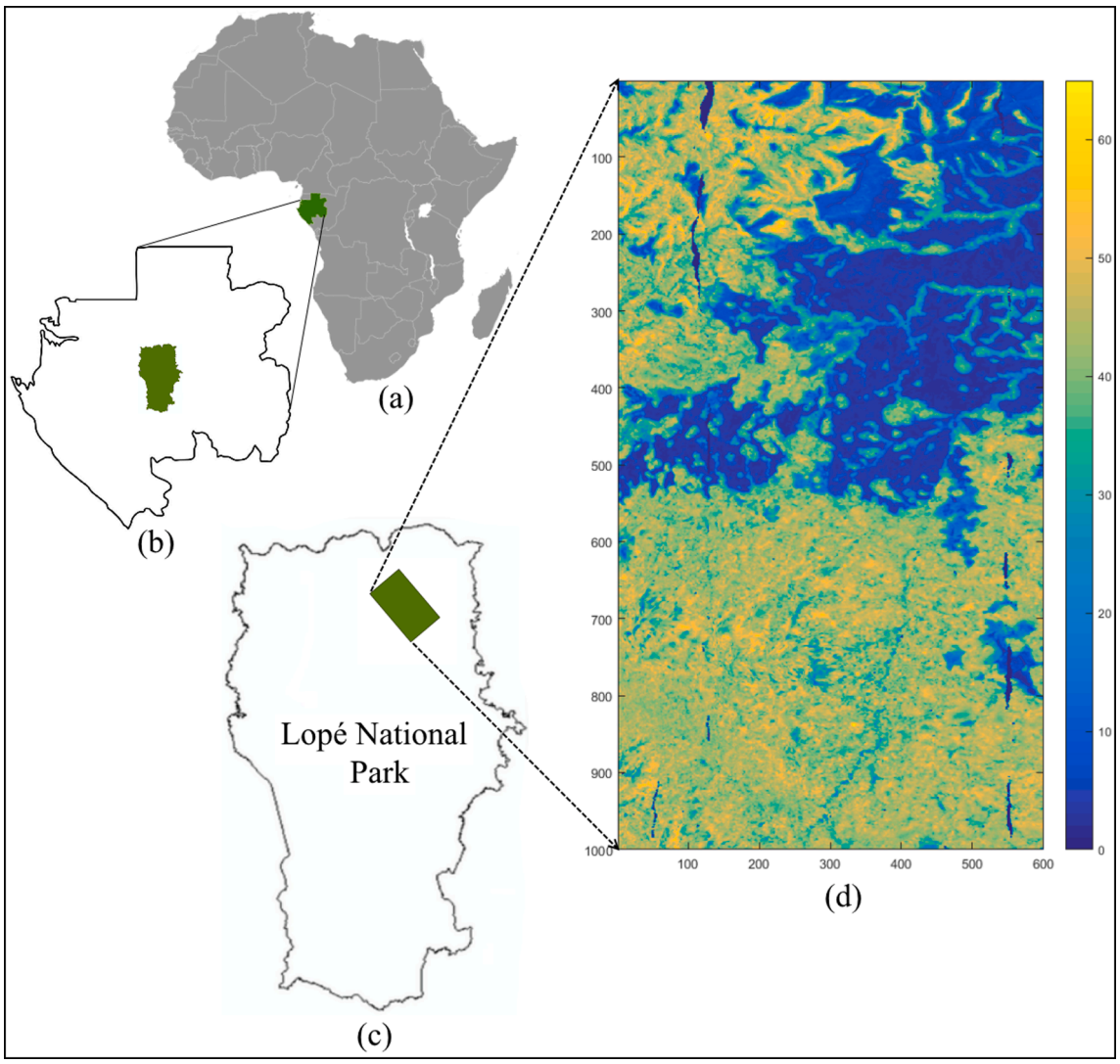

Fig. 1. (a) Location of Gabon within the continent of Africa, (b) geographical position of Lope National Park in Gabon, (c) location of study site in North Eastern part of Lope and (d) map of forest top canopy height retrieved from airborne LiDAR (RH100).

2. Study site and data

The datasets used for this study was acquired as part of the AfriSAR campaign (ESA, 2017). The campaign was organised by the European Space Agency and NASA to collect a series of airborne and field data at multiple forest sites in Gabon namely: Mondah, Lope, Mabounie and Rabi (ESA, 2017). Here, we focus on Lope.

2.1. Study site

The study site is located at the North Eastern part of Lope National Park in central Gabon (Fig. 1). The area covers three dominant vegetation types, namely short/sparse savannas (0–20 m), vegetation with mid-range height (20–40 m) and tall/dense forest (20–60 m). Fig. 1 (a) is the location of Gabon within the continent of Africa, Fig. 1 (b) represents the geographical position of Lope National Park in Gabon, Fig. 1 (c) is the location of study site in North Eastern part of Lope and Fig. 1 (d) is the map of forest top canopy height retrieved from airborne LiDAR (RH100). The RH100 map indicates three dominant regions within the study site:

i) Dark blue areas are the non-vegetated, bare soils, and sparsely distributed short woody savannas, where the canopy height reaches up to 20 m. This area covers about 40% of the test site;
ii) Light blues areas are vegetation with medium range height (20–40 m). They only cover about 20% of the test site and mainly located at the edge between the non-vegetated and forested regions; and
iii) Green/light yellow areas are tall/dense forested regions with canopy height ranges between 40 and 60 m. They cover about 40% of the test site. These areas comprise trees with different ages: young (<10 years), intermediate (10–24 years), older (25–49 years), maturing (>50 years) and old growth and various tropical species (Lewis and Labrière, 2016).

The topographic variation is visible within the test site which is more dominant in the north part of the image.

2.2. Radar acquisitions

Fully polarimetric SAR data were acquired by the NASA's UAVSAR, which is an airborne instrument equipped with an L band SAR and operates at 1217.5–1297.5 MHz (Lavalle and Hensley, 2012). The UAVSAR dataset for Lope was collected in February 2016. The nominal

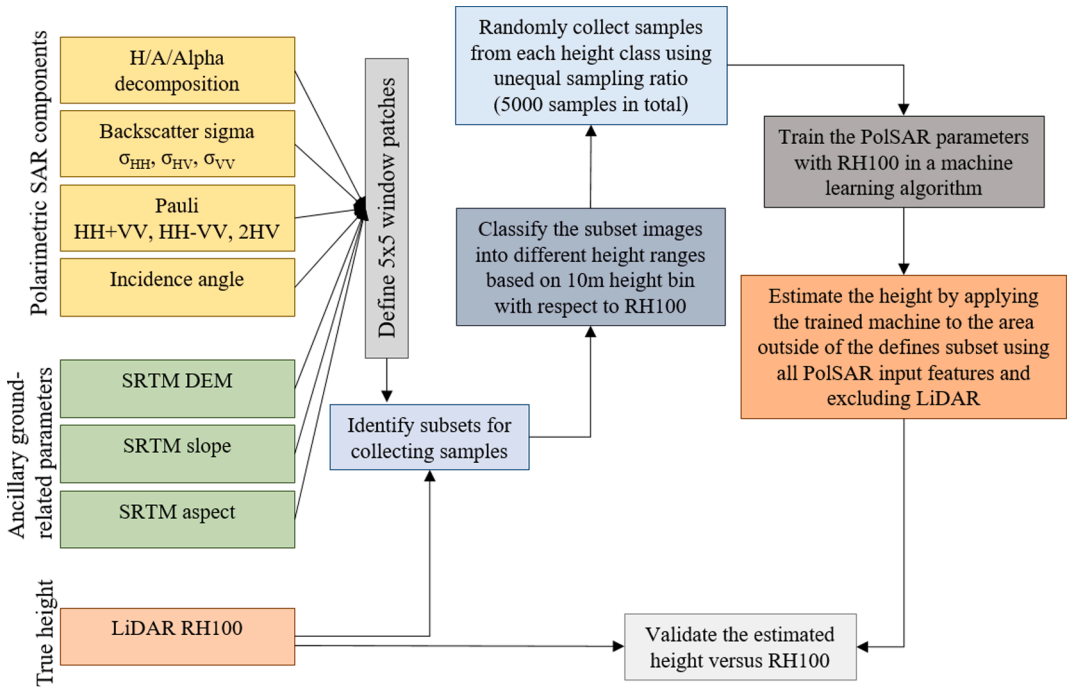

Fig. 2. Overview of methodology followed in this research. There are seven key stages: 1) generating polarimetric SAR components, 2) defining a 5x5 window patches to reduce the noise, 3) identifying couple of subsets for samples collection, 4) collecting samples, 5) training the algorithm, 6) applying the trained algorithm to the area outside of subsets to estimate the height and 7) validating the results versus true height.

flight altitude was 12.5 km, which allowed a data coverage of about 22 km wide. The incidence angles range from $\theta = 25^{\circ}$ to $\theta = 65^{\circ}$ from near to far range. The UAVSAR polarimetric single-look-complex (SLC) data has ground range and azimuth resolutions of 2.5 m and 1 m, respectively (Lavalle and Hensley, 2012, Hensley et al., 2009)

2.3. LiDAR acquisitions

LiDAR data were acquired by the Land Vegetation and Ice Sensor (LVIS) LiDAR sensor (Anderson et al., 2008). LVIS is an airborne mounted sensor on the NASA Langley KingAir B-200. LVIS nominal footprint diameter is 25 m with 9 m separation along track. The LVIS waveforms allow a retrieval of various metrics and relative height ranges. In this study we used the LVIS relative height 100 (RH100) which refers to forest top canopy height. RH100 was produced and distributed by the GSFC LVIS team. The raster image of RH100 datasets was provided in slant range geometry with a dimension of 600x1000 (pixels). LiDAR data was co-registered with UAVSAR image using location information stored in the LVIS metadata (Pourshamsi et al., 2018a). The original dimensions of UAVSAR SLC image were 3000 × 29000 pixels. The UAVSAR image was multi-looked using a window of 5 × 29 to have it in the same geometry of the LiDAR image. The LVIS and UAVSAR images cover the same area (Fig. 1). Nevertheless, for the data integration, only 5000 samples (less than 1%) of the LiDAR collected across a small subset of the scene are used for training the algorithm; the remaining pixels are used for validating the results.

3. Methodology

An overview of methodology followed in this research is given in Fig. 2.

3.1. Polarimetric SAR processing

The method starts with generating a set of PolSAR variables by decomposing the 2 × 2 polarimetric complex scattering matrix. We used Pauli basis target vector, H/A/Alpha polarimetric target decompositions (Cloude and Pottier, 1996), and backscattering which will be briefly illustrated in the following. Out of many available decomposition techniques, the H/A/Alpha method was selected as its components have shown significant potential for forest ecosystem monitoring applications. However, their potentials for forest height estimations have been poorly investigated in the scientific literature. Pourshamsi et al., (2018b) made a brief exploration of this approach by using different decomposition techniques including H/A/Alpha (Cloude and Pottier, 1996) and Krogager (Krogager, 1990). Pourshamsi et al., (2018c) further investigated this, and revealed that including PolSAR parameters generated by both decomposition techniques does not significantly improve the accuracy of the estimated height but just increase the data processing time. Therefore, in the current study we only use H/A/Alpha components (Cloude and Pottier, 1996).

3.1.1. H/A/alpha decomposition

This decomposition technique was developed by Cloude and Pottier (Cloude and Pottier, 1996). Entropy (H), alpha (α) and anisotropy (A) are the polarimetric components of this decomposition. They are effective components which provide important information behind the scattering mechanism inside each pixel of a SAR image. It is based on an eigenvalue–eigenvector decomposition of a coherency matrix T_3. The types of scattering processes are identified by the eigenvectors, and their relative magnitude is given by their eigenvalue (Cloude and Pottier, 1996). The components of this decompositions are alpha (α), entropy (H) and anisotropy (A). Alpha angle (α) is the main component which identifies the principal scattering mechanism. Entropy (H) measures the statistical disorder of individual scatterer inside a pixel. Anisotropy (A) is paired with entropy (H) and measures the relative significance of the secondary scattering mechanisms (Cloude and Pottier, 1996). A low value of entropy result in a noisy anisotropy. When entropy values are high, the types of scattering processes become indistinguishable. Hence, anisotropy supports entropy for identifying the number of distinguishable scatterers (Cloude and Pottier, 1996).

Table 1
Input features used for training machine learning algorithms.

Input Parameters	**SAR Based**	**Backscatter in dB (σ_0)**			
		σ_{HH}	σ_{HV}	σ_{VV}	
		Pauli basis target vectors			
		HH + VV	HH-VV	2HV	
		H/A/Alpha decomposition components			
		Entropy (H)	alpha (α)	anisotropy (A)	
	Ancillary datasets	**Ancillary datasets**			
		SRTM DEM	STRM slope	STRM aspect	Incidence angle
	LiDAR Based	**Forest top canopy height**			
		RH100			

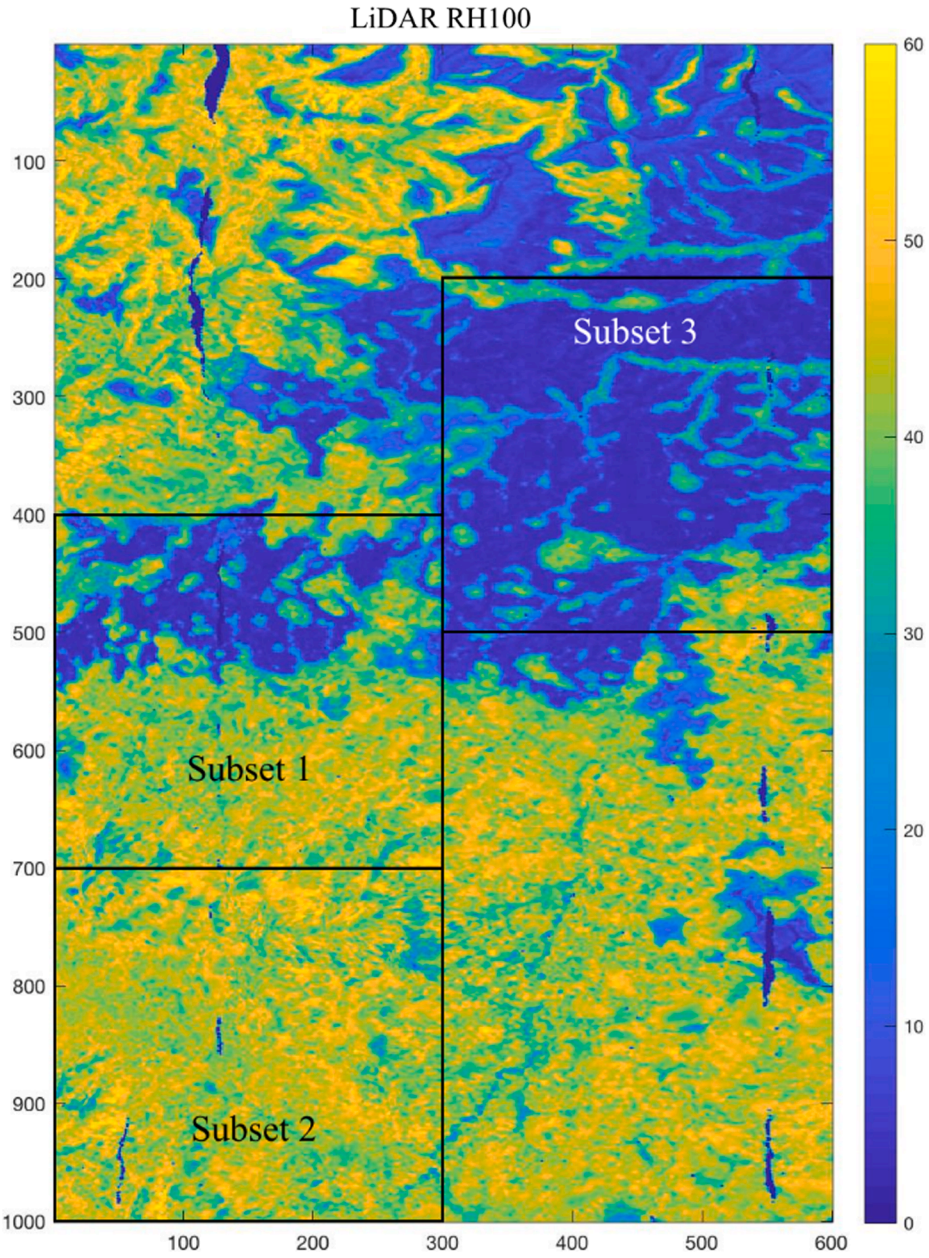

Fig. 3. Identification of multiple subsets for collecting samples.

3.1.2. Backscattering parameters

The radar backscatter coefficient (σ_0) is the signal reflected back to the sensor by the scattering elements of an illuminated scene, and provides information on the surface parameters such as geometric shape, dielectric properties of the target and roughness (Oliver and Quegan, 2004, Wallington and Woodhouse, 2006, Ulaby et al., 2014). The backscatter information is influenced by different radar parameters such as polarisation, incidence angle and frequency of the incident radiation. We calculated the backscatter coefficient (σ_0) in dB for all available polarisations (i.e. HH, HV and VV) using the following formula:

Table 2
Number of training samples categorized in three different height ranges collected from different subsets.

Height Range [m]	Subset 1	Subset 2	Subset 3
0–20	1172	148	3578
20–40	1610	1166	1071
40–60	2218	3686	351

$$\sigma_0\ (\mathrm{dB}) = 10{*}\log_{10}(|backscatter|) \quad (1)$$

where $|backscatter|$ is the absolute value of single look complex image.

We followed the procedures given above and generated the polarimetric SAR components. In addition to these, the incidence angle, SRTM Digital Elevation Model (DEM), SRTM aspect and SRTM slope were used for input features. The total list of polarimetric SAR parameters and ancillary components are gathered in Table 1.

3.2. Sampling scenario

3.2.1. Sample size

The random sampling technique was followed to collect the required training samples. In total, 5000 samples were selected which is less than 1% of the entire image (600,000 pixels). The samples were collected across three different height classes [0–20 m, 20–40 m, 40–60 m], according to the RH100 image, using an unequal sampling ratio driven by the proportion of each height class in the RH100 image.

Furthermore, the patch size (5 × 5) was utilized to extend the features dimension and to reduce the biased error of the estimation. Thus, the number of features for each sample used for training and estimation is 5 × 5 × 16 = 400 (16 is the number of input training features).

3.2.2. Sample types

To assess the dependence of the algorithms on the training data, three groups of training samples were selected (subset 1, 2 and 3 in

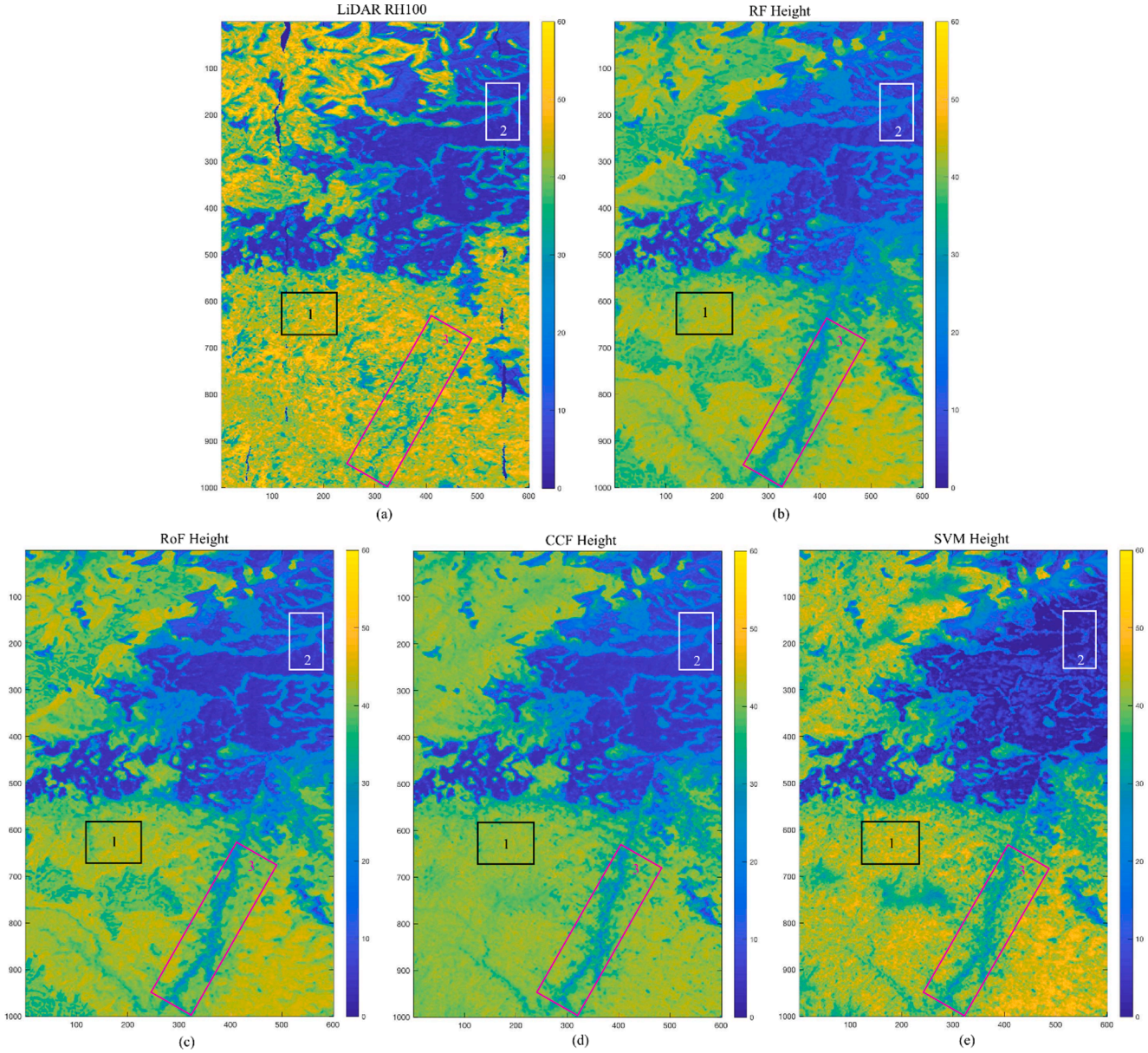

Fig. 4. The estimated heights from different algorithms based on samples collected from subset 1. Subset 1 includes features both from non-vegetated and highly vegetated regions. Image (a) is the height derived from LiDAR RH100. Image (b) is the estimated height from Random Forest (RF), image (c) from Rotation Forest (RoF), image (d) from Canonical Correlation Forest (CCF), and image (e) is from Support Vector Machine (SVM).

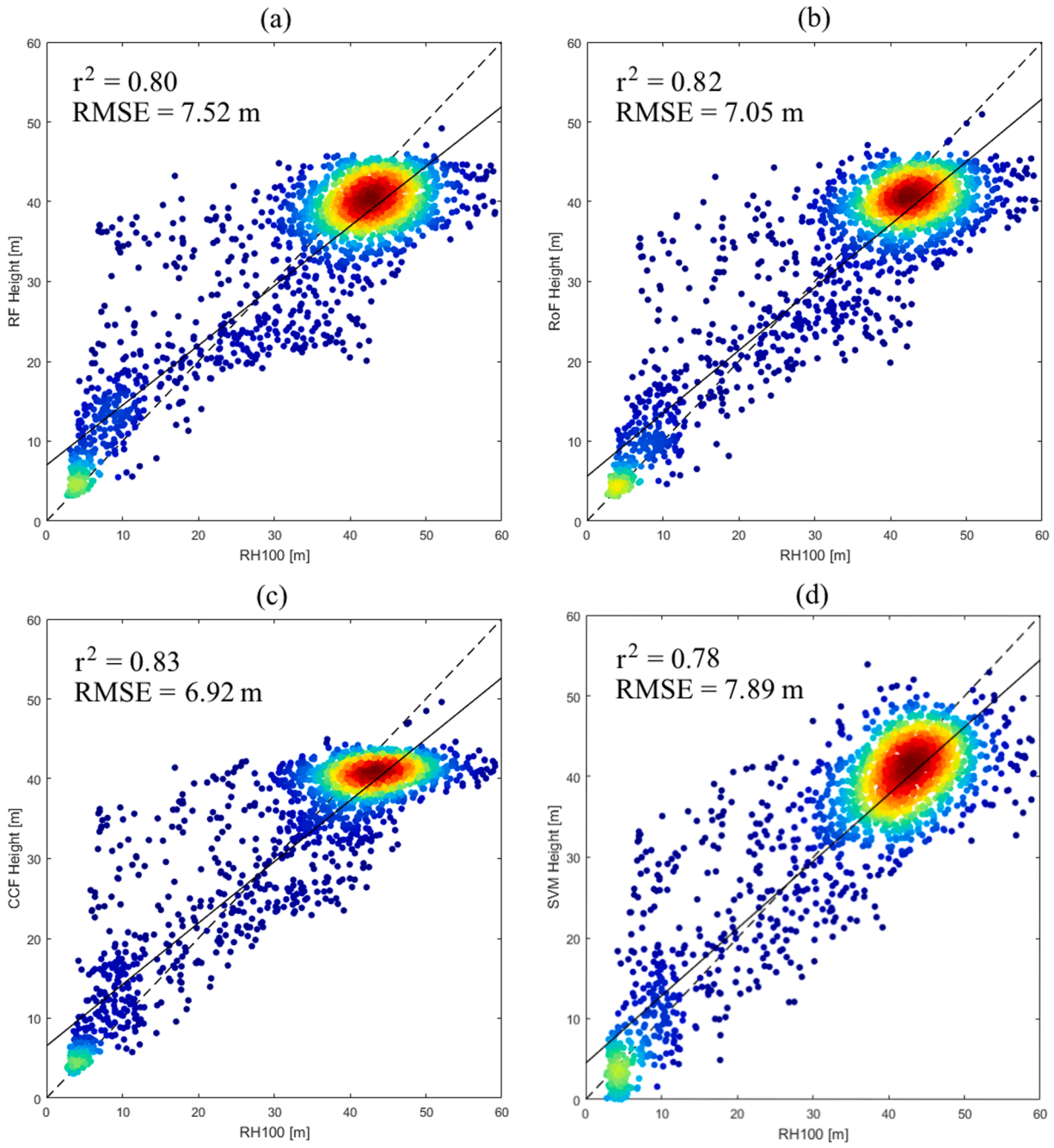

Fig. 5. Validations plots for individual algorithms versus LiDAR RH100 for the heights estimated based on samples collected from subset 1. a) validation of the height estimated from Random Forest (RF), b) from Rotation Forest (RoF), c) from Canonical Correlation Forest (CCF), and d) is from Support Vector Machine (SVM).

Fig. 3). Table 2 lists the training samples from different height classes across three subsets. Subset 1 represents the diversity of features within the test site. It includes non-vegetated regions together with vegetation with different height ranges short/sparse (0–20 m), mid-range height (20–40 m) and tall/dense (40–60 m).

The distribution of samples from the different classes is relatively similar to 1172 samples from 0 to 20 m class, 1610 from 20 to 40 m, and 2218 from 40 to 60 m (Fig. 3 and Table 2).

Subset 2 represents the forested region of the study site. The features are mainly from medium (20–40 m) and large (40–60 m) height classes. Out of the total 5000 samples, only 148 samples belong to short height class 0–20 m, whereas 1166 samples are from 20 to 40 m and 3686 ones from 40 to 60 m (Fig. 3 and Table 2).

Subset 3 represents the non-vegetated and short/sparse vegetation features of the study site. There are 3578 samples from 0 to 20 m height class, 1071 from 20 to 40 m, and only 351 from 40 to 60 m (Fig. 3 and Table 2).

3.3. Machine learning algorithms

We used DT ensemble and SVM classifier to integrate LiDAR and PolSAR components.

3.3.1. Desision tree ensmble

DT ensemble consists of a series of T trees $\{\xi_1(X), \ldots, \xi_T(X)\}$ where $\{X, Y\} = \{(x_1, y_1), \ldots, (x_n, y_n)\}$ are the total number of n training samples. $\times$ denotes D-dimensional features (F) obtained from PolSAR parameters and ancillary datasets and y is the forest top canopy height

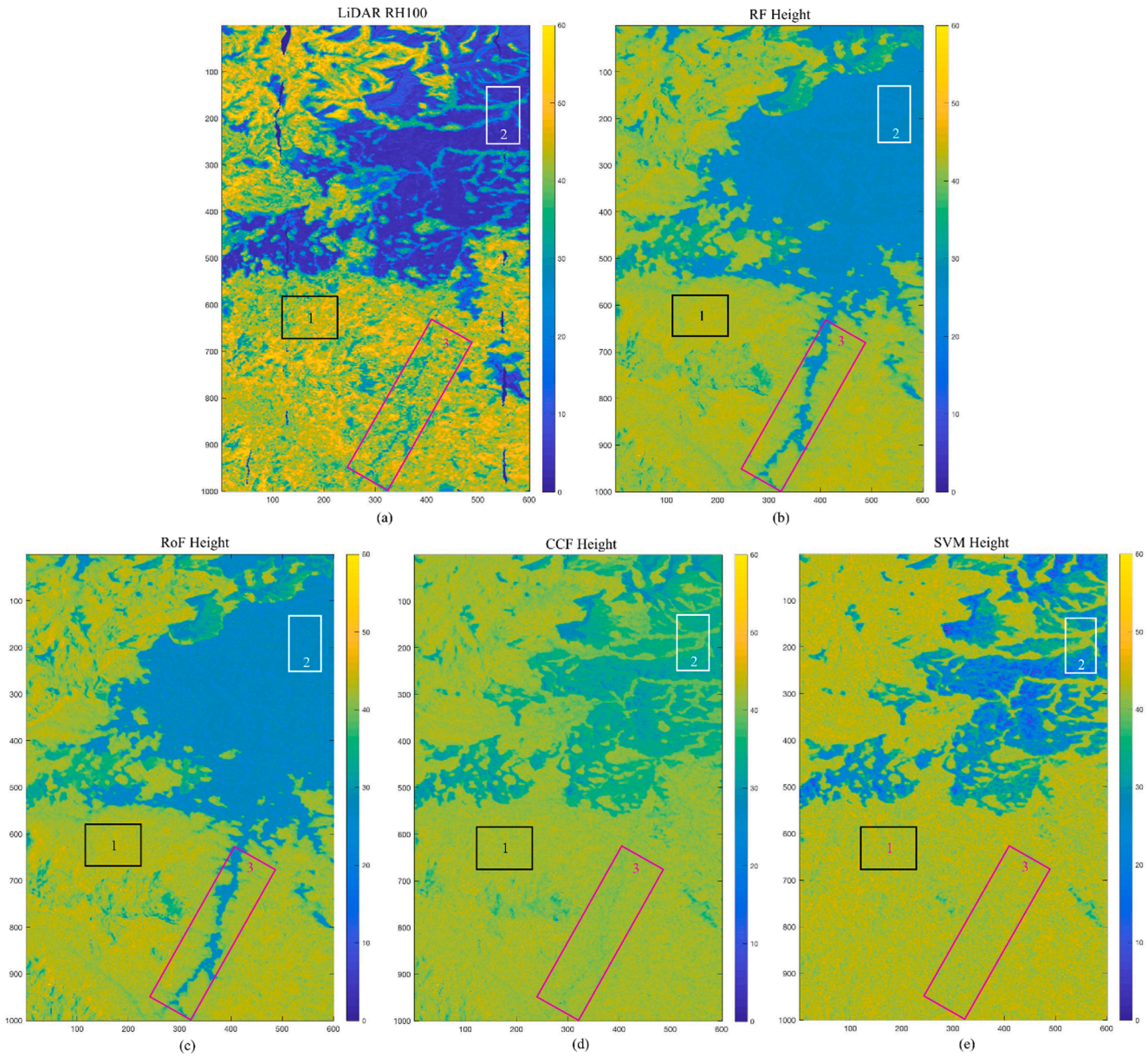

Fig. 6. The estimated heights from different algorithms based on samples collected from subset 2. Subset 2 includes features from highly vegetated regions where the trees height ranges between 20 and 60 m. Image (a) is the height derived from LiDAR RH100. Image (b) is the estimated height from Random Forest (RF), image (c) from Rotation Forest (RoF), image (d) from Canonical Correlation Forest (CCF), and image (e) is from Support Vector Machine (SVM).

(RH100) acquired from LiDAR. In this work, D equals to 400 which is obtained by applying a 5×5 window to 16 input features. The final output is obtained by averaging all tree predictors. To construct the diverse decision trees, three ensemble methods, RF (Breiman, 2001), RoF (Rodriguez et al., 2006) and CCF (Rainforth and Wood, 2015) are applied.

3.3.2. Support vector machine

For SVM classifier, the following regression function $g(x)$ is learned:

$$g(x) = \langle W, \varnothing(x) \rangle + b \tag{4}$$

where w is the weight vector in the kernel feature space, $\varnothing(x)$ is the kernel feature mapping of x, and b is the bias. The solution is obtained by solving a convex optimization problem. Where LiDAR and PolSAR components are not linearly separable, a non-linear modeling can be achieved by means of the 'kernel trick', which maps the data into a higher dimensional space. We used a Radial Basis Function (RBF) kernel to model the non-linear relationship between the RH100 and the polarimetric SAR features. The kernel's bandwidth (h) and regularization parameter (λ) control the RBF. The possible overfitting issue is avoided by deciding optimal values for the parameters using a grid search method with a 10-fold cross validation approach (Smola and Schölkopf, 2004, Pelckmans et al., 2005).

4. Results and discussion

The results are divided into three different sections corresponding each subset that is used for selection of training samples (refer to Section 3.2.2). Subset 1 presents the diversity of features within the test site and covers various height ranges (0–60 m); Subset 2 is located within tall/dense forested areas with height ranges mainly between 40 and 60 m; and Subset 3 includes non-vegetated and short/sparse vegetation with height ranges between 0 and 20 m (Table 2).

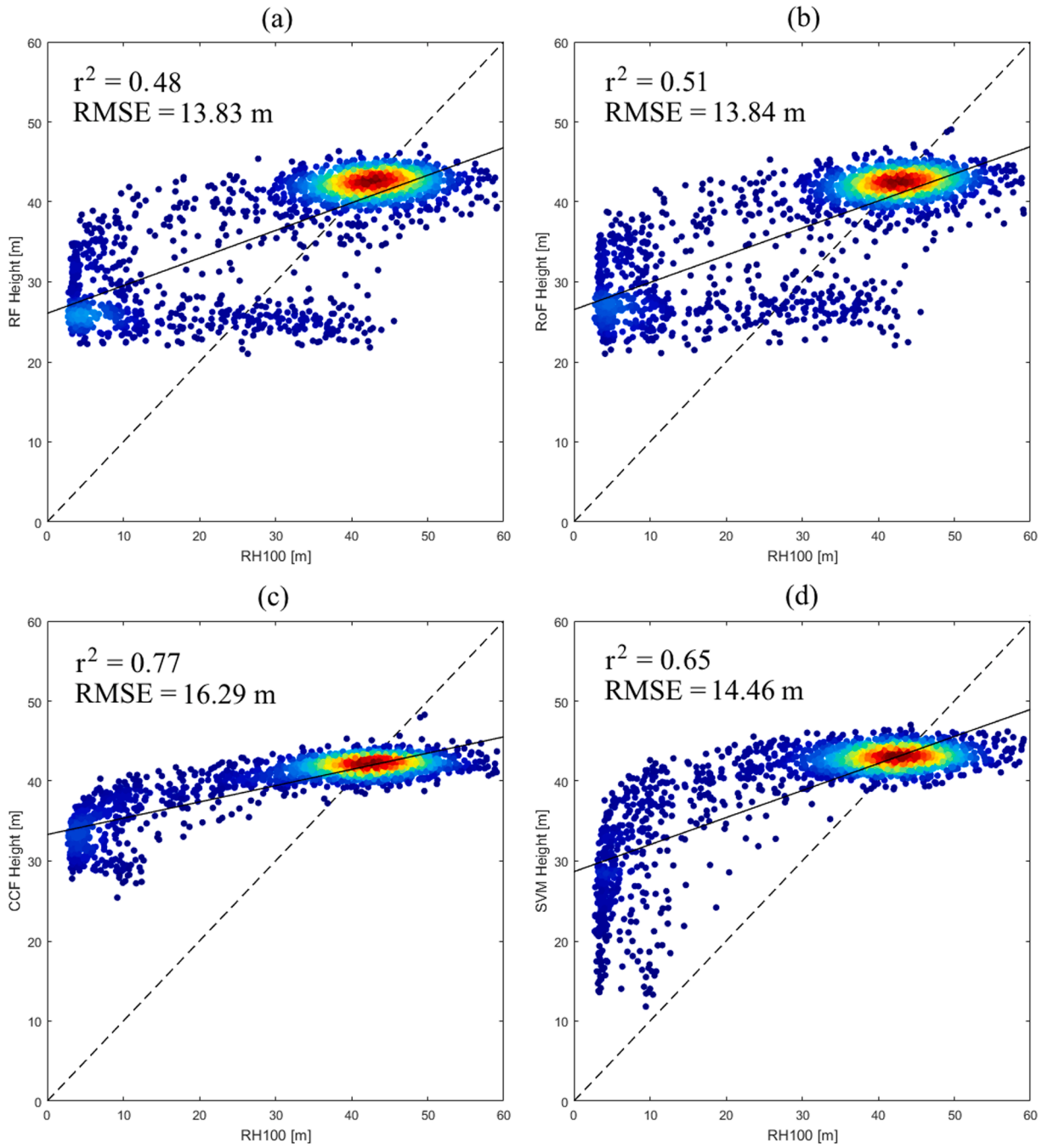

Fig. 7. Validations plots for individual algorithms versus LiDAR RH100 for the heights estimated based on samples collected from subset 2. a) validation of the height estimated from Random Forest (RF), b) from Rotation Forest (RoF), c) from Canonical Correlation Forest (CCF), and d) is from Support Vector Machine (SVM).

4.1. Subset 1

Fig. 4 indicates the map of estimated heights from the different algorithms used. The validation scatterplots for each algorithm are presented in Fig. 5. Overall, the accuracy of estimated heights is good with R^2 0.80, 0.82, 0.83, and 0.78; and RMSE of 7.52, 7.05, 6.92, and 7.89 m for RF, RoF, CCF and SVM respectively. Different algorithms performed relatively similar, SVM worked slightly better for tall/dense forest (40–60 m) and CCF for short/sparse vegetation (0–20 m). The results for mid-range height (20–40 m) are similar between all algorithms with slightly overestimation.

To better judge the performance of the models, we have identified three typical regions within the test site (Fig. 4). Box 1 is selected from the forested (40–60 m), box 2 is within non-vegetated to short/sparse vegetation (0–20 m), and box 3 includes vegetation with mid-range height (20–40 m). There is slight underestimation of height for box 1 using RF, RoF and CCF, with better result performed by SVM. For box 2 with short vegetation, RF, RoF and CCF performed quite well with better performance from CCF, while SVM did not perform as well as others. This could be observed also in Fig. 5 (d). The performance of all algorithms is relatively similar for box 3 where all underestimate the vegetation heights.

4.2. Subset 2

Fig. 6 indicates the map of estimated heights from different algorithms. The validation scatterplots for different algorithms are presented in Fig. 7.

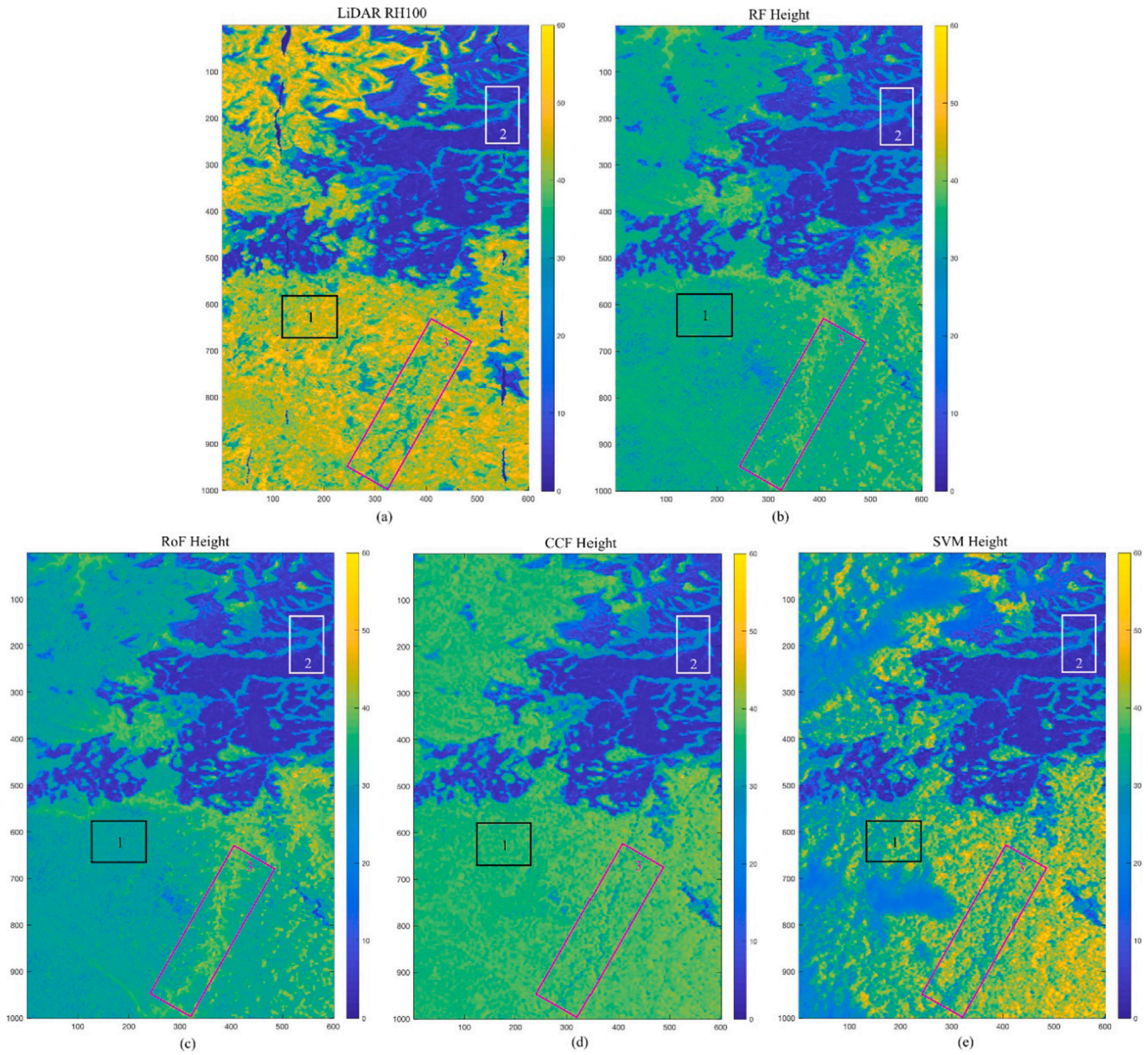

Fig. 8. The estimated heights from different algorithms based on samples collected from subset 3. Subset 3 includes features mainly from non-vegetated and short/sparse vegetation. Image (a) is the estimated height from Random Forest (RF), image (b) from Rotation Forest (RoF), image (c) from Canonical Correlation Forest (CCF), and image (d) is from Support Vector Machine (SVM).

The accuracy of estimated heights is similar for all the algorithms for heights above 40 m. The R^2 0.48, 0.51, 0.77, and 0.65 for RF, RoF, CCF and SVM respectively. In the same order the calculated RMSE is 13.83, 13.84, 16.29, and 14.46 m. The large values of RMSE reports the large overestimation of the height for height ranges between 0 and 40 m. This is clearly due to the lack of samples from these height classes. For tall vegetation (40–60 m), all algorithms performed similar, but CCF and SVM resulted in higher R^2 (Fig. 7). According to the identified regions (Fig. 6) within the test site, for box 1 (40–60 m), the estimated heights from all the algorithms are similarly underestimated. For box 2 with short vegetation, RF and RoF did not perform well and they even did not capture the pattern of features on the ground. CCF and SVM captured the pattern but the estimated height is somewhat overestimated. In opposite, for box 3 (20–40 m), RF and RoF could capture the pattern with overestimated height, while CCF and SVM did not perform well at all. Despite the relatively high r^2, the results are not good, and saturation could be observed.

4.3. Subset 3

Fig. 8 indicates the map of estimated heights from different algorithms. The validation scatterplots for different algorithms are presented in Fig. 9. The accuracy of estimated heights is pretty good for heights below 20 m. The R^2 0.72, 0.71, 0.77, and 0.54; and RMSE of 9.29, 9.81, 7.54, and 10.81 m for RF, RoF, CCF and SVM respectively. The large values of RMSE reports the large underestimation of the height for height ranges above 40 m. This is clearly due to the lack of samples from these height classes. For short vegetation (0–20 m), all algorithms performed relatively well with CCF and SVM worked slightly better.

According to the identified regions (Fig. 8) within the test site, for box 1 (40–60 m), the heights are fairly underestimated by all algorithms. For box 2 with short vegetation, all performed really well with RF and RoF slightly better. For box 3 (20–40 m), CCF and SVM performed slightly better in compare to RF and RoF. While CCF resulted in the scatterplot with the least dispersion, it is clear a saturation point for the

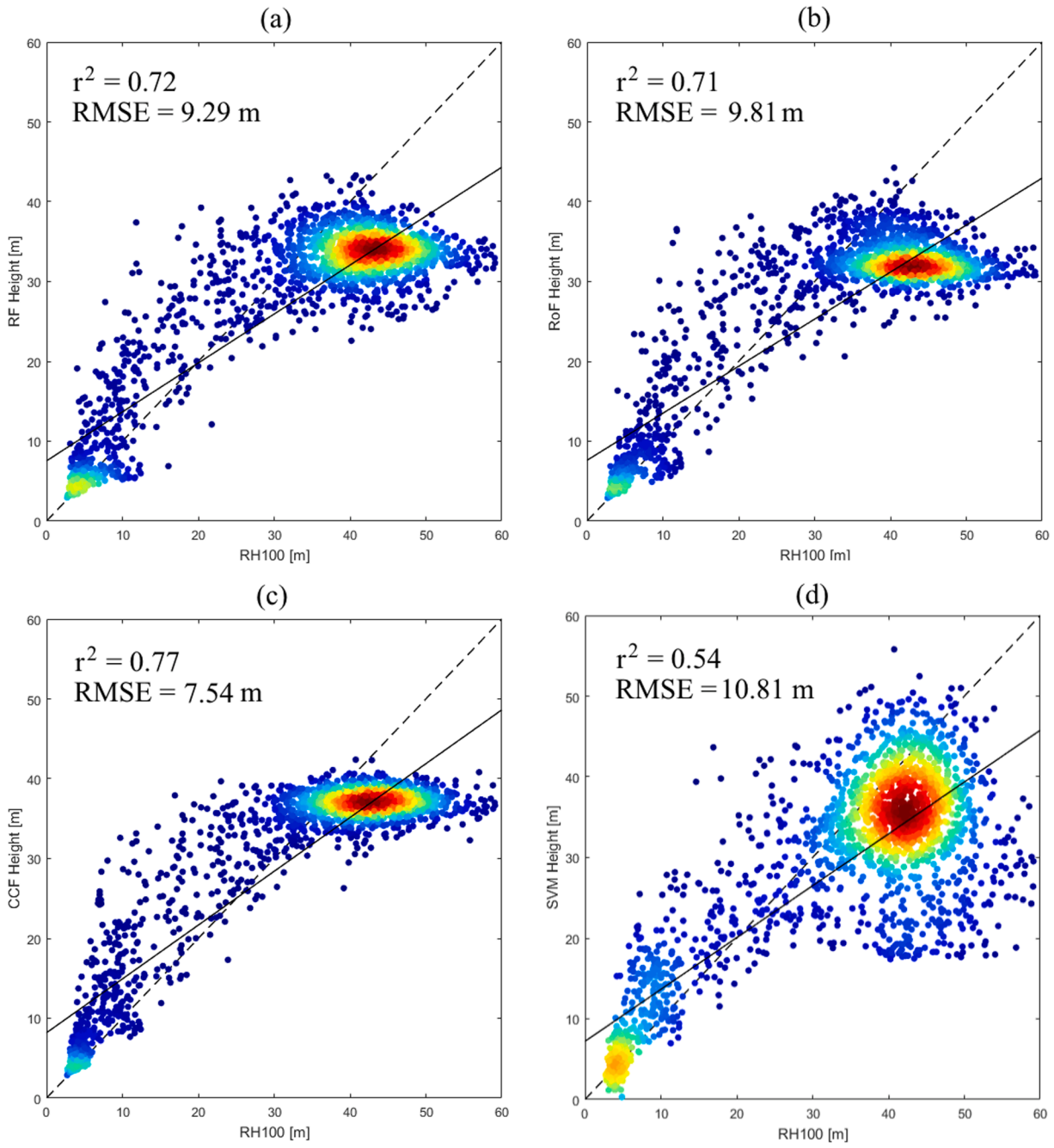

Fig. 9. Validations plots for individual algorithms versus LiDAR RH100 for the heights estimated based on samples collected from subset 3. a) validation of the height estimated from Random Forest (RF), b) from Rotation Forest (RoF), c) from Canonical Correlation Forest (CCF), and d) is from Support Vector Machine (SVM).

upper lobe. This saturation is less evident in RF and RoF; and SVM seems to work better, generally. The reason for the saturation of RF, RoF and CCF, is because RF (and its derived algorithms) cannot predict values beyond the maximum and minimum values found in the training data, which is clearly seen in the scatterplots, whereas SVM can extrapolate values, although it is patent the large uncertainty of estimates outside the range of values of the training data (Smola and Schölkopf, 2004, Pelckmans et al., 2005).

In general, different machine learning algorithms were applied to confirm the potential of this approach for estimating forest height from PolSAR parameters. The motivation is not on comparing how different machine algorithms are performing but indicating that PolSAR parameters are capable of estimating forest height, and they are not limited to a specific type of machine learning algorithm.

4.4. Model dependence on the selected training data

The results achieved from subset 1 have higher accuracy in compare to the other two subsets. To better compare the results obtained based on samples collected from different subsets, we generated the map of height differences by subtracting the estimated height of individual algorithms from RH100. Fig. 10 reports the histograms of these. For subset 1, a similar amount of overestimation and underestimation of height (~-17 to + 17 m) is observed for all algorithms. For subset 2, a large overestimation of height (~10–35 m) are observed, while for subset 3, an underestimation of height (~17 m) and small overestimation (~5 m) are noticeable.

In subset 1, the training samples cover the different height classes harmoniously, 23% of samples comes from 0 to 20 m, 32.2% from 20 to

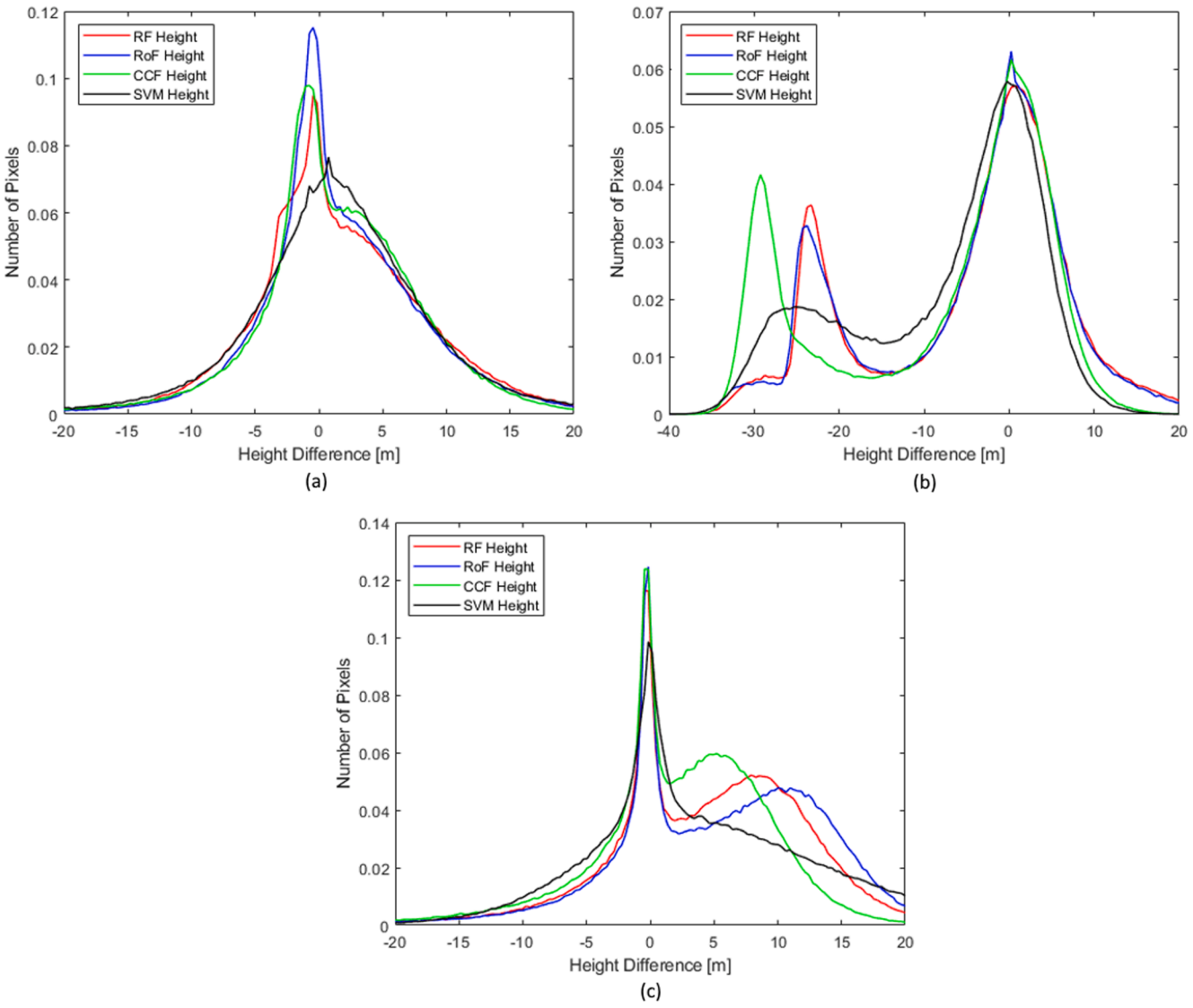

Fig. 10. (a) Histograms of height differences for individual algorithms RF, RoF, CCF and SVM based on samples collected from subset 1, (b) based on subset 2, and (c) based on subset 3; the x-axes represent the height differences with positive values signify the overestimation, and negative ones do the underestimation; the y-axes represent the number of pixels [$\times 10^6$]. Red curves stand for estimated height from RF, blue from RoF, green from CCF, and black from SVM. (For interpretation of the references to colour in this figure legend, the reader is referred to the web version of this article.)

40 m and 44.3% from 40 to 60 m. Based on the results (Fig. 10 (a)), the height is overestimated up to 17 m for mid-range height (20–40 m) and about 17 m underestimated for larger heights (40–60 m). Subset 2 covers mostly tall vegetation (40–60 m), and the training samples are mainly from this class. Only 2.9% comes from height class 0–20 m, 23.3% from 20 to 40 m and about 73.7% from 40 to 60 m. Obviously with having most samples coming from this class, the height would be well estimated for taller vegetation, and a very small amount of underestimation (~5 m) is observed. Due to the lack of training samples from shorter vegetation, the height is largely overestimated (Fig. 10 (b)). The samples collected from subset 3 mostly come from short height with 71.5% from height class 0–20 m, 21.4% from 20 to 40 m and only 7% from 40 to 60 m. As expected, the height is well estimated for shorter vegetation, and it is underestimated about (~17 m) for taller vegetation (Fig. 10 (c)).

According to the results, the performance of the machine learning models is highly dependent on the training data. The tall heights (40–60 m) are largely underestimated when the samples are from subset 3, and short heights (0–20 m) are overestimated when the samples are picked from subset 2. The mid-range heights (20–40 m) are commonly overestimated in all the subsets. This is due to the lack of training samples from this height class. In general, the test site includes a small number of vegetation with mid-range height.

The tall heights are slightly underestimated when the samples are collected from subset 2 which are mainly have tall height samples. This could be due to the canopy-penetrating capabilities of L-band SAR. The forest height in Lope is high (up to 60 m). The L-band SAR might not able to penetrate the canopy completely and reach the ground. In such case, the bottom part of the trees remains unseen and might cause underestimation of the height. The other reason could be related to the topographic effect inside the UAVSAR images. This effect was corrected using the SRTM DEM. However, the coarse resolution of the SRTM (30 $\times$ 30 m) might not be sufficient for correcting terrain affect inside the high-resolution UAVSAR image (2.5 $\times$ 1 m). Topographic effects are visible within the Lope site. Therefore, the height might be underestimated on negative slope and overestimated on positive slopes (Kugler et al., 2015).

Table 3
Contribution of individual input features in the model performance (their effects appearance in number of pixels).

Subset 1	Subset 2	Subset 3
Entropy (3210)	Entropy (2630)	Slope (1026)
Slope (760)	Slope (370)	Alpha (800)
Alpha (130)	Anisotropy (250)	Entropy (760)
Anisotropy (76)	σ_{HV} (113)	DEM (750)
DEM (53)	2HV (110)	Aspect (640)
HH-VV (53)	HH-VV (50)	Anisotropy (620)
Incidence Angle (45)	DEM (50)	Incidence Angle (560)
2HV (44)	Incidence Angle (45)	HH-VV (550)
σ_{HV} (42)	Aspect (42)	HH + VV (445)
HH + VV (41)	HH + VV (40)	σ_{VV} (400)
σ_{HH} (36)	Alpha (40)	σ_{HH} (390)
aspect (33)	σ_{VV} (36)	σ_{HV} (328)
σ_{VV} (32)	σ_{HH} (35)	2HV (326)

4.5. *The sensitiveness of polarimetric features to canopy height estimation*

We carried out features importance analysis to understand the sensitiveness of individual input features to canopy height estimation (Table 3). The sensitivity of individual input features varies from one subset to another. The top four important components in RF algorithm for each subset by order of importance are as follow:

- Subset 1: entropy (H), slope, alpha (α) and anisotropy (A)
- Subset 2: entropy (H), slope, anisotropy (A), σ_{HV}
- Subset 3: slope, alpha (α), entropy (H), DEM

The components of the H/A/alpha decomposition together with slope are significantly sensitive. However, their sensitiveness varies depending on the selected training samples. Slope is the key component in all scenarios. This is due to the effects of topography and terrain slope within the test site. In a flatter test site, this parameter should have less impact.

The significant sensitivity of H/A/alpha decomposition components are related to different types of scattering occurred inside one pixel with respect to different features on the ground (Fig. 11). Various features on the ground interact differently with the radar beam (Cloude and Pottier, 1996).

These various scattering scenarios with respect to different features on the ground will make different values for H/A/Alpha components (Fig. 12).

Different values of these components will cause a different level of sensitivity of them to the forest canopy height estimation. Where there are medium values of alpha and entropy with lower values of anisotropy, the scatterings represent the dense vegetation with taller heights (40–60 m). This is due to volume scattering which causes a large amount of radar beam to be scattered away from the senor, and only a small amount bounced back to it. In this case, the values of all components are at the medium. In contrast, higher values of entropy and alpha with low values of anisotropy are due to double bounce scattering. This represents sparse/short vegetation (0–20 m) where the radar beam reaches the ground, and the reflected signal may hit tree trunks and bounce back towards the sensor. In comparison, the low values of alpha and entropy with higher values of anisotropy can be representative of non-vegetated region and bare soil where the radar beam reaches the ground and immediately bounce away from the senor and they show very small sensitivity to the canopy height. What becomes more apparent here is the range of variation: for short/sparse vegetation, anisotropy and entropy vary in a much larger range than for tall/dense vegetation. This is due to the fact that over sparse/short vegetation, there is a mixture of different scattering mechanisms, surface, volume and double bounce, whereas over the tall/dense forested regions, volume scattering is more dominant and over non-vegetated region surface scattering (Cloude and Pottier, 1996).

Entropy is a sensitive parameter in all cases with higher sensitivity when samples are collected from subset 1 and 2. Entropy measures the statistical disorder of different scattering mechanisms within each pixel. These phenomena more likely appears within forested region which causes higher values for entropy. When entropy values are high, the types of scattering processes become indistinguishable which makes it hard to differentiate between multiple scattering processes incurred over dense forest (subset 2 and part of subset 1). Hence, anisotropy supports entropy for identifying the number of distinguishable scatterers.

In non-vegetated areas, entropy values are low which result in a noisy anisotropy. Hence, the different types of scattering processes

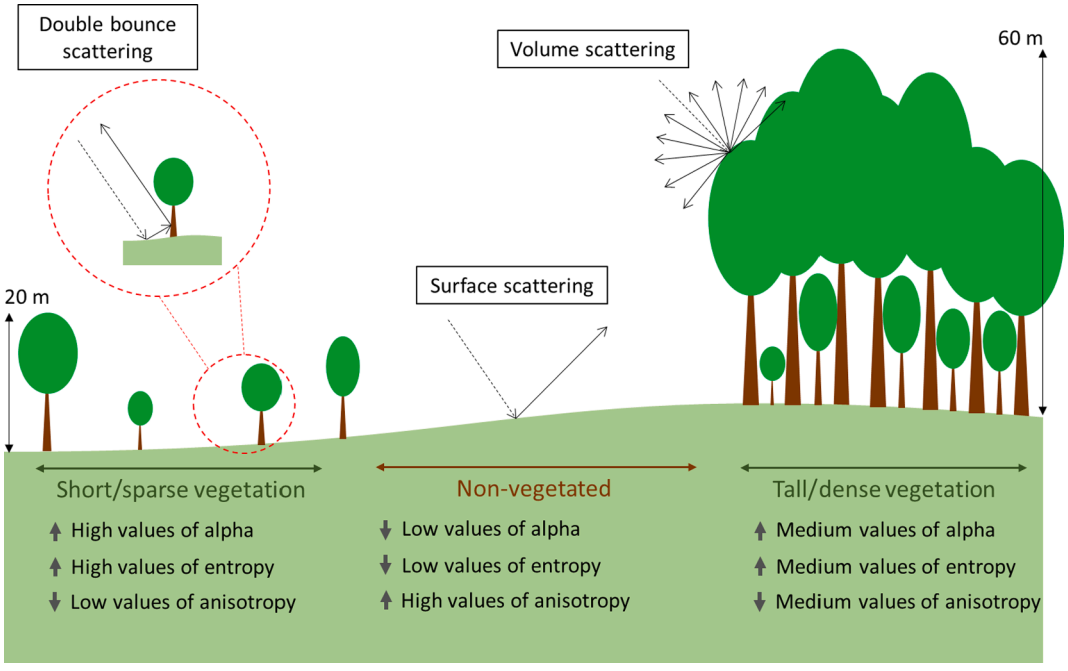

Fig. 11. A simulation of different features within the test site and possible contribution of individual PolSAR components.

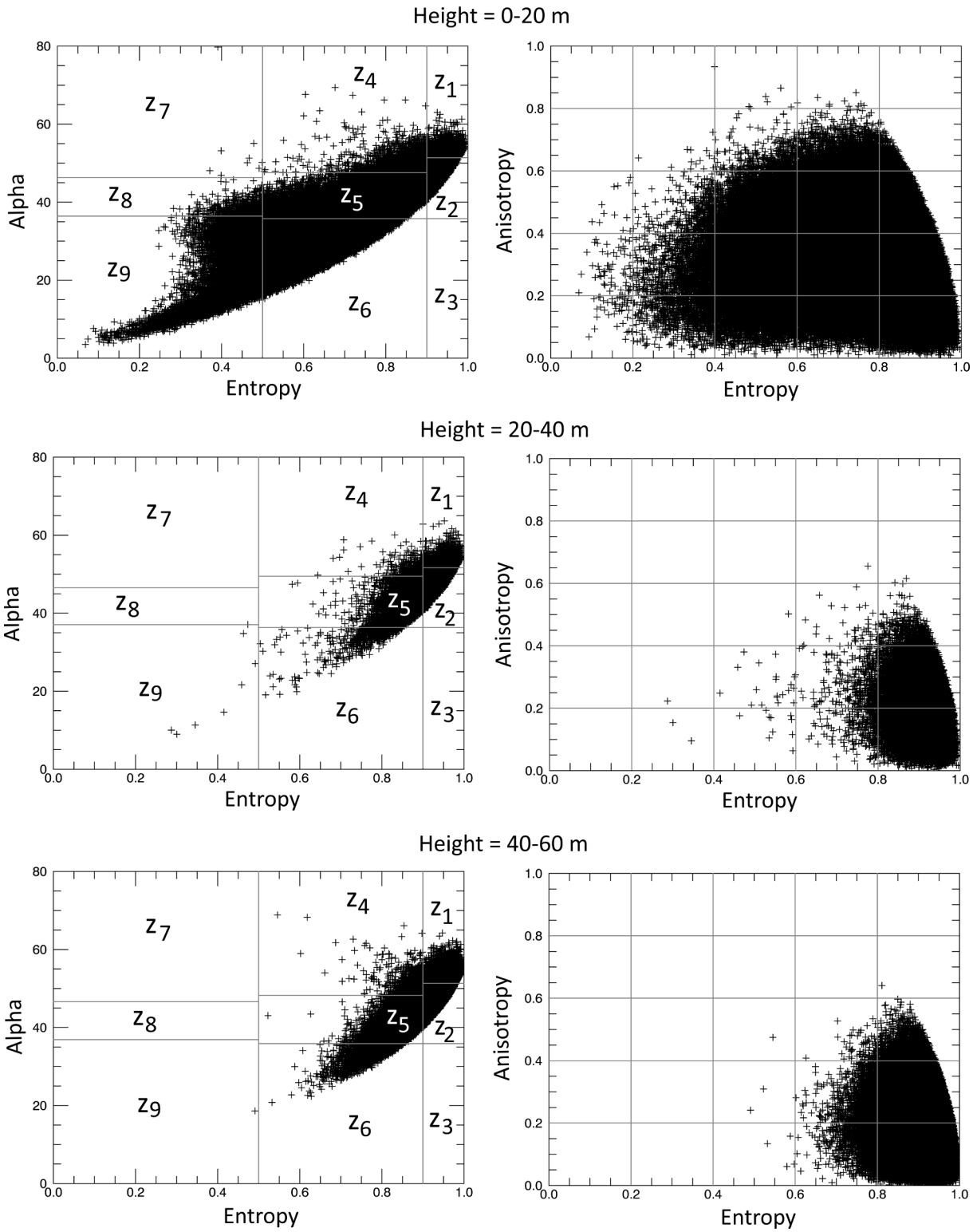

Fig. 12. Analysis of H/A/alpha components for different height ranges within the study site. Left: entropy/alpha (H/alpha) two-dimensional classification plane, right: entropy/anisotropy (H/A) two-dimensional classification plane.

become indistinguishable. This is why entropy and anisotropy have lower sensitivity to canopy height estimation when the training samples are selected from subset 3 which mainly covers non-vegetated area.

Additionally, the sensitivity of other components should be taken into account. When the training samples are selected from subset 2, HV, σ_{HV} and Pauli 2HV show a large sensitivity due to the presence of volume scattering. In compare, when the training samples are selected from subset 3, Pauli HH-VV and HH + VV are sensitive which are representative of ground scattering.

The polarimetric SAR components represent two-dimensional information about the scattering mechanisms. It is not possible to derive three-dimensional details from them. So, LiDAR with its vertical information could be included in the machine learning algorithms to enable retrieval of three-dimensional information. They allocate the canopy top

height provided by LiDAR to corresponding polarimetric SAR scattering processes and define a relationship between them within a specified subset. The defined relation between input features can then be used to estimate height in an area outside of the subset. Having samples collected from a small subset for training, the results are relatively good. Nevertheless, the results are very dependent of diversity of input samples. The collected samples are from a small subset from a certain part of the scene. This, however, could not represent all the features with the entire test site. Improving the samples adequately for collecting input training samples can capture the height variations and can potentially increase the accuracy of the results.

5. Conclusions

We have shown the capability of PolSAR parameters for forest height estimation using machine learning algorithms. We integrated LiDAR samples and multiple PolSAR variables extracted from different polarimetric decomposition techniques using different machine learning algorithms including RFs, RoFs, CCFs and SVMs. Each algorithm was run three times with the training samples were selected from a subset of the scene representing different vegetation characteristics. The first set of training samples were chosen from a heterogeneous part which covers various height ranges (0–60 m); second ones are within the forested part with high heights (40–60 m); and the third ones are from a part which mostly cover short heights (0–20 m). Whilst the results have shown a great potential of PolSAR variables for retrieval of forest height, the algorithm performance highly depend on the input training samples. The best results were achieved when the training samples are selected from the heterogeneous part of the scene which includes vegetation with different height ranges and density. Therefore, for successful height estimation over a heterogeneous forest, the input features should convey a set of different features within the study site. Different machine learning algorithms were used for the experiment, RF, RoF, CCF and SVM. Whilst the results are pretty similar, SVM performed slightly better. The results confirm that it is possible to estimate forest height using PolSAR parameters together with a small portion of LiDAR samples in the absence of interferometric measurements. This presented way of combining PolSAR parameters and LiDAR for forest height estimation is beneficial for the upcoming and current data from spaceborne SAR and LiDAR missions (BIOMASS, NISAR and GEDI) which provide a wealth amount of polarimetric SAR and LiDAR data at global scale.

Declaration of Competing Interest

The authors declare that they have no known competing financial interests or personal relationships that could have appeared to influence the work reported in this paper.

Acknowledgment

This research work has been carried out as part of Maryam Pourshamsi's PhD during an internship at Geoinformatics Unit, RIKEN Center for Advanced Intelligence Project (AIP), Tokyo. Her PhD is sponsored by Engineering and Physical Science Research Council (EPSRC), grant reference: EP/M508081/1.

References

Anderson, J.E., Plourde, L.C., Martin, M.E., Braswell, B.H., Smith, M.-L., Dubayah, R.O., Hofton, M.A., Blair, J.B., 2008. Integrating waveform lidar with hyperspectral imagery for inventory of a northern temperate forest. Remote Sens. Environ. 112, 1856–1870.

Breiman, L. 2001. Random forests. Machine learning, 45, 5-32.

Brigot, G., Simard, M., Colin-Koeniguer, E., Boulch, A., 2019. Retrieval of Forest Vertical Structure from PolInSAR Data by Machine Learning Using LIDAR-Derived Features. Remote Sensing 11 (4), 381.

Chen, G., Hay, G.J., St-Onge, B., 2012. A GEOBIA framework to estimate forest parameters from lidar transects, Quickbird imagery and machine learning: A case study in Quebec, Canada. Int. J. Appl. Earth Obs. Geoinf. 15, 28–37.

CLOUDE, S. R. & PAPATHANASSIOU, K. P. Coherence optimisation in polarimetric SAR interferometry. IGARSS'97. 1997 IEEE International Geoscience and Remote Sensing Symposium Proceedings. Remote Sensing-A Scientific Vision for Sustainable Development, 1997. IEEE, 1932-1934.

Cloude, S.R., Papathanassiou, K.P., 1998. Polarimetric SAR interferometry. IEEE Trans. Geosci. Remote Sens. 36, 1551–1565.

Cloude, S.R., Pottier, E., 1996. A review of target decomposition theorems in radar polarimetry. IEEE Trans. Geosci. Remote Sens. 34, 498–518.

Dubayah, R.O., Drake, J.B., 2000. Lidar remote sensing for forestry. J. Forest. 98, 44–46.

ESA 2017. Technical Assistance For The Development Of Airborne SAR And Geophysical Measurements During The Afrisar Experiment.

Fassnacht, F.E., Hartig, F., Latifi, H., Berger, C., Hernández, J., Corvalán, P., Koch, B., 2014. Importance of sample size, data type and prediction method for remote sensing-based estimations of aboveground forest biomass. Remote Sens. Environ. 154, 102–114.

Fayad, I., Baghdadi, N., Bailly, J.S., Barbier, N., Gond, V., Hérault, B., El Hajj, M., Fabre, F., Perrin, J., 2016. Regional scale rain-forest height mapping using regression-kriging of spaceborne and airborne LiDAR data: Application on French Guiana. Remote Sensing 8 (3), 240.

García, M., Saatchi, S., Ustin, S., Balzter, H., 2018. Modelling forest canopy height by integrating airborne LiDAR samples with satellite Radar and multispectral imagery. Int. J. Appl. Earth Obs. Geoinf. 66, 159–173.

Gleason, C.J., Im, J., 2012. Forest biomass estimation from airborne LiDAR data using machine learning approaches. Remote Sens. Environ. 125, 80–91.

Gu, C., Clevers, J.G., Liu, X., Tian, X., Li, Z., Li, Z., 2018. Predicting forest height using the GOST, Landsat 7 ETM+, and airborne LiDAR for sloping terrains in the Greater Khingan Mountains of China. ISPRS J. Photogramm. Remote Sens. 137, 97–111.

HENSLEY, S., ZEBKER, H., JONES, C., MICHEL, T., MUELLERSCHOEN, R. & CHAPMAN, B. First deformation results using the NASA/JPL UAVSAR instrument. 2009 2nd Asian-Pacific Conference on Synthetic Aperture Radar, 2009. IEEE, 1051-1055.

Khati, U., Singh, G., Kumar, S., 2018. Potential of Space-Borne PolInSAR for Forest Canopy Height Estimation Over India—A Case Study Using Fully PolarimetricL-, C-, andX-Band SAR Data. IEEE J. Sel. Top. Appl. Earth Obs. Remote Sens. 11 (7), 2406–2416.

Krieger, G., Moreira, A., Fiedler, H., Hajnsek, I., Werner, M., Younis, M., Zink, M., 2007. TanDEM-X: A satellite formation for high-resolution SAR interferometry. IEEE Trans. Geosci. Remote Sens. 45, 3317–3341.

Krogager, E., 1990. New decomposition of the radar target scattering matrix. Electron. Lett. 26, 1525–1527.

Kugler, F., Lee, S.-K., Hajnsek, I., Papathanassiou, K.P., 2015. Forest height estimation by means of Pol-InSAR data inversion: The role of the vertical wavenumber. IEEE Trans. Geosci. Remote Sens. 53, 5294–5311.

LAVALLE, M. & HENSLEY, S. Demonstration of repeat-pass POLINSAR using UAVSAR: The RMOG model. 2012 IEEE International Geoscience and Remote Sensing Symposium, 2012. IEEE, 5876-5879.

Lee, J.-S., Pottier, E., 2009. Polarimetric radar imaging: from basics to applications. CRC Press.

Lewis, S. and Labrière, N., 2016. Report for AfriSAR Gabon in situ field campaign.

Li, W., Niu, Z., Shang, R., Qin, Y., Wang, L., Chen, H., 2020. High-resolution mapping of forest canopy height using machine learning by coupling ICESat-2 LiDAR with Sentinel-1, Sentinel-2 and Landsat-8 data. Int. J. Appl. Earth Obs. Geoinf. 92, 102163.

Oliver, C., Quegan, S., 2004. Understanding synthetic aperture radar images. SciTech Publishing.

Pelckmans, K., de Brabanter, J., Suykens, J.A., de Moor, B., 2005. Handling missing values in support vector machine classifiers. Neural Networks 18, 684–692.

Pourshamsi, M., Garcia, M., Lavalle, M., Balzter, H., 2018a. A Machine-Learning Approach to PolInSAR and LiDAR Data Fusion for Improved Tropical Forest Canopy Height Estimation Using NASA AfriSAR Campaign Data. IEEE J. Sel. Top. Appl. Earth Obs. Remote Sens. 11, 3453–3463.

POURSHAMSI, M., GARCIA, M., LAVALLE, M., POTTIER, E. & BALZTER, H. Machine-Learning Fusion of Polsar and Lidar Data for Tropical Forest Canopy Height Estimation. IGARSS 2018-2018 IEEE International Geoscience and Remote Sensing Symposium, 2018b. IEEE, 8108-8111.

Pourshamsi, M., Garcia, M., Lavalle, M., Pottier, E., Balzter, H., 2018c. Machine-Learning Fusion of Polsar and Lidar Data for Tropical Forest Canopy Height Estimation. ESA EO Science Conference.

RAINFORTH, T. & WOOD, F. 2015. Canonical correlation forests. arXiv preprint arXiv: 1507.05444.

Rodriguez, J.J., Kuncheva, L.I., Alonso, C.J., 2006. Rotation forest: A new classifier ensemble method. IEEE Trans. Pattern Anal. Mach. Intell. 28, 1619–1630.

Shimada, M., Itoh, T., Motooka, T., Watanabe, M., Shiraishi, T., Thapa, R., Lucas, R., 2014. New global forest/non-forest maps from ALOS PALSAR data (2007–2010). Remote Sens. Environ. 155, 13–31.

Silva, C.A., Saatchi, S., Garcia, M., Labriere, N., Klauberg, C., Ferraz, A., Meyer, V., Jeffery, K.J., Abernethy, K., White, L., Zhao, K., 2018. Comparison of small-and large-footprint lidar characterization of tropical forest aboveground structure and biomass: A case study from central gabon. IEEE J. Select. Topics Appl. Earth Observ. Remote Sens. 11 (10), 3512–3526. In press.

Simard, M., Pinto, N., Fisher, J.B., Baccini, A., 2011. Mapping forest canopy height globally with spaceborne lidar. J. Geophys. Res. Biogeosci. 116 (G4).

Singh, S.K., Srivastava, P.K., Gupta, M., Thakur, J.K., Mukherjee, S., 2014. Appraisal of land use/land cover of mangrove forest ecosystem using support vector machine. Environmental earth sciences 71 (5), 2245–2255.

Smola, A.J., Schölkopf, B., 2004. A tutorial on support vector regression. Statistics and computing 14, 199–222.

Stojanova, D., Panov, P., Gjorgjioski, V., Kobler, A., Džeroski, S., 2010. Estimating vegetation height and canopy cover from remotely sensed data with machine learning. Ecol. Inf. 5 (4), 256–266.

Torres, R., Snoeij, P., Geudtner, D., Bibby, D., Davidson, M., Attema, E., Potin, P., Rommen, B., Floury, N., Brown, M., 2012. GMES Sentinel-1 mission. Remote Sens. Environ. 120, 9–24.

ULABY, F. T., LONG, D. G., BLACKWELL, W. J., ELACHI, C., FUNG, A. K., RUF, C., SARABANDI, K., ZEBKER, H. A. & VAN ZYL, J. 2014. Microwave radar and radiometric remote sensing, University of Michigan Press Ann Arbor.

Wallington, E.D., Woodhouse, I.H., 2006. Forest height retrieval from commercial X-band SAR products. IEEE Trans. Geosci. Remote Sens. 44, 863–870.

Wang, H., Zhao, Y., Pu, R., Zhang, Z., 2015. Mapping Robinia pseudoacacia forest health conditions by using combined spectral, spatial, and textural information extracted from IKONOS imagery and random forest classifier. remote Sensing 7 (7), 9020–9044.

Xie, Y., Fu, H., Zhu, J., Wang, C., Xie, Q., 2019. A LiDAR-Aided Multibaseline PolInSAR Method for Forest Height Estimation: With Emphasis on Dual-Baseline Selection. IEEE Geoscience and Remote Sensing Letters.

Zhao, J., Zhang, Z., Han, S., Qu, C., Yuan, Z., Zhang, D., 2011. SVM based forest fire detection using static and dynamic features. Computer Science and Information Systems 8 (3), 821–841.